Photorhabdus luminescens Toxins ADP-Ribosylate Actin and RhoA to Force Actin Clustering

Alexander E. Lang *et al.*

Science **327**, 1139 (2010);
DOI: 10.1126/science.1184557

Science (print ISSN 0036-8075; online ISSN 1095-9203) is published weekly, except the last week in December, by the American Association for the Advancement of Science, 1200 New York Avenue NW, Washington, DC 20005.

3C) or TNF-α (Fig. 3D). Stimulus-dependent degradation of UbcH5c also occurred, but only in response to IL-1 and not to TNF-α (Fig. 3, C and D, and fig. S4, A and C). Knockdown of A20 with small interfering RNA (siRNA) prevented the degradation of both Ubc13 and UbcH5c (Fig. 3, C and D). However, the E3 ubiquitin ligases RNF11 and Itch were both dispensable for Ubc13 degradation, despite the requirement of Itch for the attenuation of TRAF6 ubiquitination (fig. S5). Ubc13 was also degraded in response to IL-1 and TNF-α in MEFs in an A20- and TAX1BP1-dependent manner (fig. S4). Finally, TNF-α and IL-1–induced Ubc13 and UbcH5c degradation was blocked by the proteasome inhibitor MG-132 (Fig. 3, E and F).

A20 inhibits RIP1 activation in the TNFR pathway through its deubiquitinase and E3 ligase activities; however, whether these activities are required for the down-regulation of Ubc13 and UbcH5c is unknown. A20 contains an N-terminal ovarian tumor (OTU) DUB domain and seven C-terminal zinc finger domains (Fig. 4A). A20-deficient MEFs were reconstituted with various Flag-tagged A20 deletion mutants to determine the domain(s) important for the degradation of Ubc13 and UbcH5c. Deletion of zinc fingers 5 through 7 had no effect on the degradation of Ubc13 or UbcH5c (Fig. 4B and fig. S6). However, deletion of zinc finger 4 (ZnF4) abrogated A20-mediated degradation of Ubc13 and UbcH5c (Fig. 4B and fig. S6), correlating with published reports on the importance of ZnF4 in A20-mediated inhibition of NF-κB (*17*). The degradation of Ubc13 and UbcH5c by A20 appeared to be specific because UbcH10 (also known as Ube2c) was not degraded in cells treated with IL-1 (fig. S6). Reconstitution studies in *A20*$^{-/-}$ MEFs revealed that wild-type A20, but not A20 C103A, disrupted the binding of TRAF6 and Ubc13 (fig. S7A). Overexpression of the deubiquitinating enzyme cylindromatosis (CYLD) exerted no effect on TRAF6 and Ubc13 binding, which suggests that CYLD uses a distinct mechanism to inhibit TRAF6 ubiquitination (fig. S7A). Similarly, A20, but not A20 C103A or CYLD, efficiently inhibited TRAF2-Ubc13 binding in TNF-α–stimulated *A20*$^{-/-}$ MEFs (fig. S7B). Although wild-type A20 interacted with endogenous Ubc13 and UbcH5c in cells stimulated with LPS or IL-1, both A20 C103A and A20 ZnF4 mutants were defective for binding to Ubc13 and UbcH5c (Fig. 4, C to E) and thus were unable to inhibit TRAF6 ubiquitination or promote Ubc13 degradation (fig. S8, A to C). A20 C103 and ZnF4 were also required for TAX1BP1 to interact with Ubc13 (fig. S8D). Furthermore, A20 deletion mutants lacking either the OTU domain or zinc fingers 4 and 5 were not associated with Ubc13 or UbcH5c (Fig. 4F). However, for TAX1BP1 binding, the OTU domain was dispensable and only ZnF4 was critical (Fig. 4, F and G) (*17*). Collectively, these results indicate that A20 ZnF4 is important for binding to TAX1BP1, whereas the OTU domain and ZnF4 are important for binding to Ubc13 and UbcH5c.

The human T cell leukemia virus type I (HTLV-I) Tax oncoprotein promotes a persistent NF-κB response, in part, by interacting with TAX1BP1 and disrupting the interactions between A20, TAX1BP1, and Itch (*5*). Because Tax interacts with Ubc13 (*18*), we hypothesized that Tax would prevent A20 from binding to Ubc13, thereby protecting Ubc13 from degradation. Indeed, Tax impaired the TNF-α–dependent interaction of A20 with Ubc13 (fig. S9A), as well as TNF-α–mediated degradation of Ubc13 (fig. S9B). Tax also prevented A20 from binding to TRAF6 in response to IL-1 stimulation (fig. S9C). The Tax point mutant Tax M22, but not Tax M47, is defective for NF-κB activation (*19*). Tax M22, but not Tax M47, failed to bind to Ubc13 (fig. S9D). Thus, Tax preserves E2:E3 enzyme complexes essential for NF-κB activation and prevents Ubc13 degradation, which is essential for Tax polyubiquitination (*18*).

The importance of A20 in limiting inflammation is underscored by the numerous human autoimmune diseases associated with polymorphisms in the A20 genomic region (*20*–*22*). A20 also functions as a tumor suppressor gene for B cell lymphomas (*23*, *24*). Our findings indicate that A20 disrupts key E2 and E3 ubiquitin enzyme complexes in both TNFR and TLR pathways. A20 binding to E2 or E3 enzymes may sterically interfere with their interactions, or alternatively A20 may directly modify E2 or E3 enzymes that antagonize their interactions.

References and Notes

1. B. Coornaert, I. Carpentier, R. Beyaert, *J. Biol. Chem.* **284**, 8217 (2009).
2. E. G. Lee *et al.*, *Science* **289**, 2350 (2000).
3. D. L. Boone *et al.*, *Nat. Immunol.* **5**, 1052 (2004).
4. N. Shembade, N. S. Harhaj, D. J. Liebl, E. W. Harhaj, *EMBO J.* **26**, 3910 (2007).
5. N. Shembade *et al.*, *Nat. Immunol.* **9**, 254 (2008).
6. N. Shembade, K. Parvatiyar, N. S. Harhaj, E. W. Harhaj, *EMBO J.* **28**, 513 (2009).
7. I. E. Wertz *et al.*, *Nature* **430**, 694 (2004).
8. B. Lamothe *et al.*, *J. Biol. Chem.* **282**, 4102 (2007).
9. T. Fukushima *et al.*, *Proc. Natl. Acad. Sci. U.S.A.* **104**, 6371 (2007).
10. M. Yamamoto *et al.*, *Nat. Immunol.* **7**, 962 (2006).
11. Z. P. Xia *et al.*, *Nature* **461**, 114 (2009).
12. C. S. Shi, J. H. Kehrl, *J. Biol. Chem.* **278**, 15429 (2003).
13. M. J. Bertrand *et al.*, *Mol. Cell* **30**, 689 (2008).
14. J. Wooff, L. Pastushok, M. Hanna, Y. Fu, W. Xiao, *FEBS Lett.* **566**, 229 (2004).
15. L. Deng *et al.*, *Cell* **103**, 351 (2000).
16. D. B. Conze, C. J. Wu, J. A. Thomas, A. Landstrom, J. D. Ashwell, *Mol. Cell. Biol.* **28**, 3538 (2008).
17. M. Klinkenberg, S. Van Huffel, K. Heyninck, R. Beyaert, *FEBS Lett.* **498**, 93 (2001).
18. N. Shembade, N. S. Harhaj, M. Yamamoto, S. Akira, E. W. Harhaj, *J. Virol.* **81**, 13735 (2007).
19. M. R. Smith, W. C. Greene, *Genes Dev.* **4**, 1875 (1990).
20. R. Dieguez-Gonzalez *et al.*, *Arthritis Res. Ther.* **11**, R42 (2009).
21. S. L. Musone *et al.*, *Nat. Genet.* **40**, 1062 (2008).
22. E. Y. Fung *et al.*, *Genes Immun.* **10**, 188 (2009).
23. M. Compagno *et al.*, *Nature* **459**, 717 (2009).
24. M. Kato *et al.*, *Nature* **459**, 712 (2009).

25. We thank S. C. Sun, L. Matesic, D. Abbott, C. Vincenz, P. Storz, R. Beyaert, and the Belgian Coordinated Collections of Microorganisms/Laboratory of Molecular Biology of Ghent University (BCCM™/LMBP) for reagents and H. Ishikawa for assistance in the preparation of BMDMs and BMDCs. The project described was supported by NIH grants RO1GM083143 and RO1CA135362 awarded to E.W.H. The content is solely the responsibility of the authors and does not necessarily represent the official views of the National Cancer Institute/National Institute of General Medical Sciences or the National Institutes of Health.

Supporting Online Material

www.sciencemag.org/cgi/content/full/327/5969/1135/DC1
Materials and Methods
Figs. S1 to S9
References

23 September 2009; accepted 14 January 2010
10.1126/science.1182364

Photorhabdus luminescens Toxins ADP-Ribosylate Actin and RhoA to Force Actin Clustering

Alexander E. Lang,[1,2]* Gudula Schmidt,[1]* Andreas Schlosser,[3] Timothy D. Hey,[4] Ignacio M. Larrinua,[4] Joel J. Sheets,[4] Hans G. Mannherz,[5,6] Klaus Aktories[1]†

The bacterium *Photorhabdus luminescens* is mutualistically associated with entomopathogenetic nematodes. These nematodes invade insect larvae and release the bacteria from their intestine, which kills the insects through the action of toxin complexes. We elucidated the mode of action of two of these insecticidal toxins from *P. luminescens*. We identified the biologically active components TccC3 and TccC5 as adenosine diphosphate (ADP)–ribosyltransferases, which modify unusual amino acids. TccC3 ADP-ribosylated threonine-148 of actin, resulting in actin polymerization. TccC5 ADP-ribosylated Rho guanosine triphosphatase proteins at glutamine-61 and glutamine-63, inducing their activation. The concerted action of both toxins inhibited phagocytosis of target insect cells and induced extensive intracellular polymerization and clustering of actin. Several human pathogenic bacteria produce related toxins.

Photorhabdus luminescens colonizes the intestine of infective entomophathogenetic nematodes from the genera *Heterorhabditis* in a symbiotic manner (*1*). The nematodes invade larvae of susceptible insects and release bacteria (*2*). The bacteria reach the insect hemocoel, inhibit insect immunity, proliferate rapidly, and kill the insect larvae usually within 2 days. After proliferation and recolonization by *P. luminescens*, the nematodes invade and kill new insect hosts. Thus, nematodes, harboring the bacteria, can be used as biological insecticides.

P. luminescens produces an array of toxins that are likely involved in pathogenicity against insect hosts and the symbiotic relationship with nematodes (*2*). One major toxin family of *P. luminescens* is the group of the Tc toxin complexes with masses of ~1 million daltons. Each complex is characterized by at least three basic types of functional components: TcA, TcB, and TcC (fig. S1) (*3*, *4*). TcA-like components appear to form tetramers and may be responsible for binding and/or translocation of the toxin complex (*5*). TcB-like components may function as a chaperone and/or a linker between TcA and TcC components (*6*). However, so far the mode of action of Tc toxins has not been understood.

Initially, we studied the effects of the toxins on the phagocytic activity of hemocytes from *Galleria mellonella* because *P. luminescens* infection alters their phagocytic activity. Treatment of hemocytes with the *Photorhabdus* toxin complex 3 (PTC3), which consists of TcdA1 and TcdB2/TccC3 (fig. S1), inhibited phagocytosis (Fig. 1A) (*7*). A similar effect was induced by the *Photorhabdus* toxin complex PTC5, which consists of TcdA1 and TcdB2/TccC5. PTC3 plus PTC5 in combination completely blocked phagocytosis (Fig. 1A). The biological activity depended on the complete toxin complex: TcdA1 or the TcdB2/TccC3 fusion protein alone was ineffective, and TcdB2/TccC5 did not influence phagocytosis in the absence of TcdA1 (Fig. 1A).

Because microfilaments are involved in phagocytic activity, we studied the effects of the toxins on the actin cytoskeleton. PTC3 caused extensive clustering of F-actin in *G. mellonella* hemocytes (Fig. 1B). Again, this effect was not observed when TcdA1 was missing or only the fusion protein TcdB2/TccC3 was applied (fig. S2A). A similar effect was observed with human HeLa cells (Fig. 1B), although it was less strong. To study the effects of TccC3 independently of TcdA1 and TcdB2, we introduced the toxin into target cells by means of the protective antigen (PA), which is the anthrax toxin binding and translocation component. Thus, a His-tag was added to TccC3, which allowed transport via PA into target cells without TcdA1 or TcdB2. His-tagged TccC3 caused the same formation of actin aggregates as observed with PTC3 (fig. S2B). Thus, the biological activity of PTC3 is located in the TccC3 component of the toxin.

PTC5 caused strong stress fiber formation but no actin clustering in *Galleria mellonella* hemocytes and in HeLa cells (Fig. 1B). Application of both PTC3 and PTC5 caused even stronger effects. The actin cytoskeleton was completely aggregated, forming star-like clusters all over the target cell. In HeLa cells, the cortical actin was redistributed, and actin clusters were also observed below the plasma membrane (Fig. 1B). Thus, both toxins induce major changes of the actin cytoskeleton, which most likely cause the inhibition of hemocyte phagocytosis.

TccC3 and TccC5 exhibit sequence similarities with adenosine diphosphate (ADP)–ribosyltransferases (*8*)—especially the "R, S, E" motif, which is typical for almost all ADP-ribosyltransferases and was also found in TccC3 and TccC5 (fig. S3). Using [^{32}P]NAD$^+$, we tested the ADP-ribosylation of proteins in lysates of cells by TccC3. An ~45 kDa protein was selectively labeled by TccC3 in lysates of insect Sf9 and human HeLa cells (fig. S4A). Because the labeled protein comigrated with actin, we directly tested the ADP-ribosylation of purified actin with TccC3 in the presence of [^{32}P]NAD$^+$ (Fig. 2A). This resulted in strong labeling of actin. ADP-ribosylation of actin was also catalyzed by the 32 kDa C-terminal fragment of TccC3, which shows sequence similarity with ADP-ribosyltransferases, indicating a harboring of the enzyme activity (Fig. 2A). Actin is also ADP-ribosylated by the family of binary ADP-ribosylating toxins, including C2 toxin from *C. botulinum* and iota toxin from *C. perfringens* (*9*). However, these toxins, which modify actin at arginine-177 (*10*), cause depolymerization and not polymerization or clustering of actin (*11*). Accordingly, TccC3 did not modify arginine-177. When actin was ADP-ribosylated by C2 toxin, addition of TccC3 and [^{32}P]NAD$^+$ further increased labeling, indicating modification at a different site (fig. S4B). C2 toxin–ADP-ribosylated actin (arginine-177) can be cleaved by neutral hydroxylamine. In contrast, actin ADP-ribosylated by TccC3 was not affected by hydroxylamine (fig. S4C).

Mass analytical data suggested modification of actin at threonine-148 or threonine-149 by TccC3 (fig. S5A). Mutation of both threonine-148 and threonine-149 to alanine of in vitro synthesized (β/γ)-actin confirmed that only threonine-148 was ADP-ribosylated by TccC3 (Fig. 2B).

Threonine-148 is located in the interaction site of actin with the actin monomer-binding protein thymosin-β4, which is involved in the sequestering of monomeric actin and prevents actin polymerization (fig. S6) (*12*). Cross-linking experiments demonstrated that ADP-ribosylation inhibited the interaction of thymosin-β4 with α-actin (Fig. 2C and fig. S7A). To quantify the effect of ADP-ribosylation, the rates of association and dissociation of thymosin-β4 to α-actin covalently modified at Cys374 by N-iodoacetyl-N′-(5-sulfo-1-naphthyl)ethylenediamine (AEDANS) before and after TccC3–ADP-ribosylation were determined by means of fast reaction kinetics (*13*). The rate constant of association of thymosin-β4 decreased from 0.97×10^6 to 0.37×10^6 M^{-1} s^{-1}, and its rate constant of dissociation increased from 3.11 to 8.5 s^{-1} for control and TccC3–ADP-ribosylated actin, respectively (fig. S7B), resulting in an eight-fold higher dissociation constant of the TccC3–ADP-ribosylated actin:thymosin-β4 complex (from 3.2 to 23 μM, under the conditions used).

Next, we studied the effects of thymosin-β4 on actin polymerization after ADP-ribosylation of actin by TccC3. Actin polymerization induced by

[1]Institut für Experimentelle und Klinische Pharmakologie und Toxikologie, Albert-Ludwigs-Universität Freiburg, 79104 Freiburg, Germany. [2]Fakultät für Biologie, Albert-Ludwigs-Universität Freiburg, 79104 Freiburg, Germany. [3]Zentrum für Biosystemanalyse, Core Facility Proteomics, Albert-Ludwigs-Universität Freiburg, 79104 Freiburg, Germany. [4]Discovery Research, Dow AgroSciences, Indianapolis, IN 46268, USA. [5]Physikalische Biochemie, Max-Planck-Institut für molekulare Physiologie, 44227 Dortmund, Germany. [6]Abteilung für Anatomie und Embryologie, Ruhr-Universität Bochum, 44801 Bochum, Germany.

*These authors contributed equally to this work.
†To whom correspondence should be addressed. E-mail: klaus.aktories@pharmakol.uni-freiburg.de

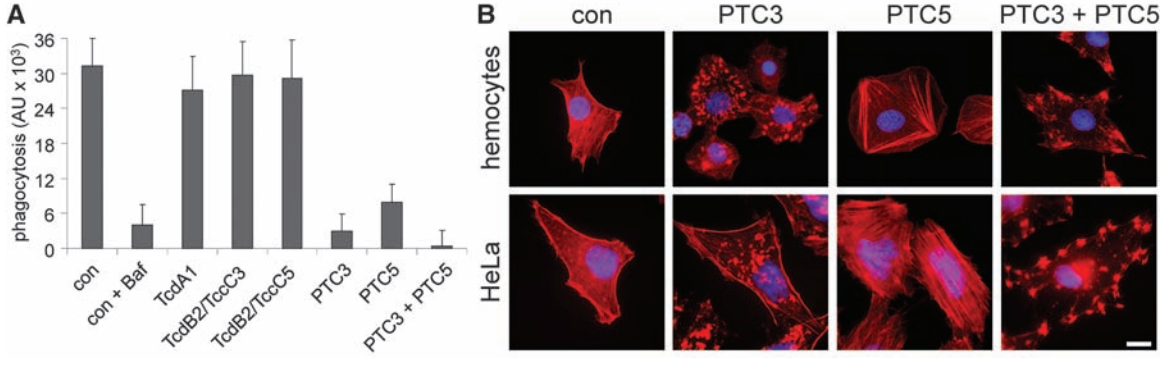

Fig. 1. Influence of *Photorhabdus* Tc proteins on phagocytosis and on the actin cytoskeleton of *G. mellonella* hemocytes and human HeLa cells. (**A**) *G. mellonella* hemocytes were treated with TcdA1, TcdB2/TccC3 or TcdB2/TccC5, PTC3 (TcdA1 + TcdB2/TccC3), or PTC5 (TcdA1 + TcdB2/TccC5) for 30 min. Phagocytosis was measured by increase in fluorescence of hemocytes. Background fluorescence was determined in the presence of bafilomycin A1 (Baf). Data are mean ± SD; $n = 3$ replicates. (**B**) *G. mellonella* hemocytes and HeLa cells were treated with the indicated toxin complexes for 2 hours (hemocytes) or 4 hours (HeLa cells). Then, the cells were fixed and stained with tetramethyl rhodamine isothiocyanate–conjugated phalloidin and 4′,6′-diamidino-2-phenylindole (scale bar, 10 μm).

addition of Mg^{2+} ions was completely prevented in the presence of equimolar thymosin-β4 (Fig. 2D). Polymerization of TccC3–ADP-ribosylated actin was faster than under control conditions. In contrast, addition of thymosin-β4 led to only a slight reduction of the initial velocity of actin polymerization but did not block polymerization of modified actin. Similar results were obtained in studies of the critical concentration of polymerization of actin (Cc) in the presence of thymosin-β4 (fig. S7C). Thus, ADP-ribosylation of actin at threonine-148 reduces the affinity of thymosin-β4 binding to actin and therefore largely eliminates actin sequestration, which may explain the observed increased intracellular content of F-actin. Cross-linking experiments of actin with profilin, which can also sequester actin (*14*), revealed that ADP-ribosylation had no or only a minor effect on the actin-profilin interaction (fig. S7D).

As shown above, PTC5 caused stress fiber formation. We studied the activity of TccC5 by means of in vitro ADP-ribosylation with [^{32}P]NAD$^+$ using insect Sf9 and human HeLa cell lysates. TccC5 catalyzed radioactive labeling of ~20 kDa proteins (Fig. 3A). Because activation of RhoA is known to induce stress fiber formation, we tested recombinant Rho guanosine triphosphatases (GTPases) as substrates of TccC5. TccC5 ADP-ribosylated RhoA and Cdc42 (Fig. 3B). The Rho isoforms RhoA, RhoB, and RhoC are well-known targets of ADP-ribosyltransferase C3 from *C. botulinum* (*15*). This modification occurs at asparagine-41 of RhoA and inhibits the biological activity of RhoA, suggesting a different target site for TccC5. To identify the site of TccC5-catalyzed ADP-ribosylation of Rho, we treated recombinant RhoA with TccC5 in the presence of NAD$^+$ and subjected peptides to mass spectrometric analysis. TccC5 ADP-ribosylated RhoA at glutamine-63 (fig. S5B). The modification site was confirmed by using the mutant proteins Q63E-RhoA or Q63L-RhoA (Q61E-Cdc42 and Q61L-Cdc42), which were not substrates of TccC5, whereas the mutants were still modified by C3 exoenzyme (Fig. 3B). Glutamine-63 of RhoA is deamidated by *Escherichia coli* cytotoxic necrotizing factor 1 (CNF1) (*16*). Accordingly, pretreatment of HeLa cells with CNF1 inhibited subsequent ADP-ribosylation by TccC5 without affecting C3-induced ADP-ribosylation at asparagine-41 (fig. S8A).

Glutamine-63 (glutamine-61 of Rac and Cdc42) plays a pivotal role in the turn-off reaction of Rho GTPases. This amino acid (or an equivalent glutamine residue) is highly conserved in G proteins and is essential for hydrolysis of GTP by the

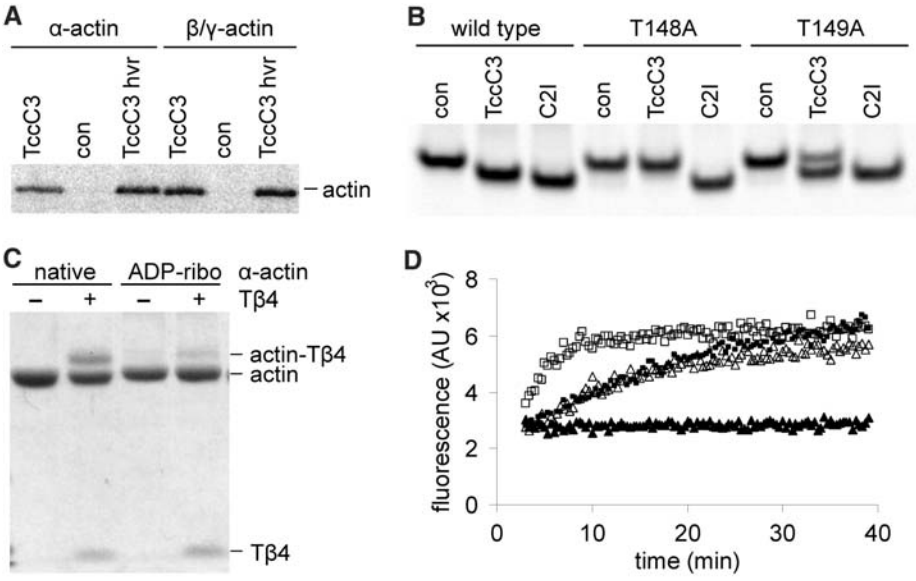

Fig. 2. ADP-ribosylation of actin by TccC3. Toxin effects on thymosin-β4 binding of actin and actin polymerization. (**A**) Purified α-actin and β/γ-actin were incubated for 45 min with [^{32}P]NAD$^+$ and TccC3 or the C-terminal (hvr) ~32 kDa fragment of TccC3. Radio-labeled proteins were detected by means of sodium dodecyl sulfate–polyacrylamide gel electrophoresis (SDS-PAGE) and phosphorimaging. (**B**) In vitro translated and [^{35}S]methionine-radiolabeled β-actin and the actin mutants T148A and T149A were ADP-ribosylated with NAD$^+$ by TccC3 or C2I. Proteins were analyzed by means of native gel electrophoresis and phosphorimaging. (**C**) Native α-actin and TccC3–ADP-ribosylated actin were cross-linked without and with thymosin-β4 (Tβ4) by 1-ethyl-3[3-(dimethylamino)-propyl]carbodiimide (EDC) and, thereafter, analyzed by means of SDS-PAGE (*24*). (**D**) Native α-actin supplemented with pyrene-actin (Δ, ▲) or TccC3–ADP-ribosylated α-actin supplemented with TccC3–ADP-ribosylated pyrene-actin (□, ■) was polymerized by the addition of $MgCl_2$ in the absence (Δ, □) or presence (▲, ■) of thymosin-β4. Polymerization was followed by the increase in pyrene-fluorescence.

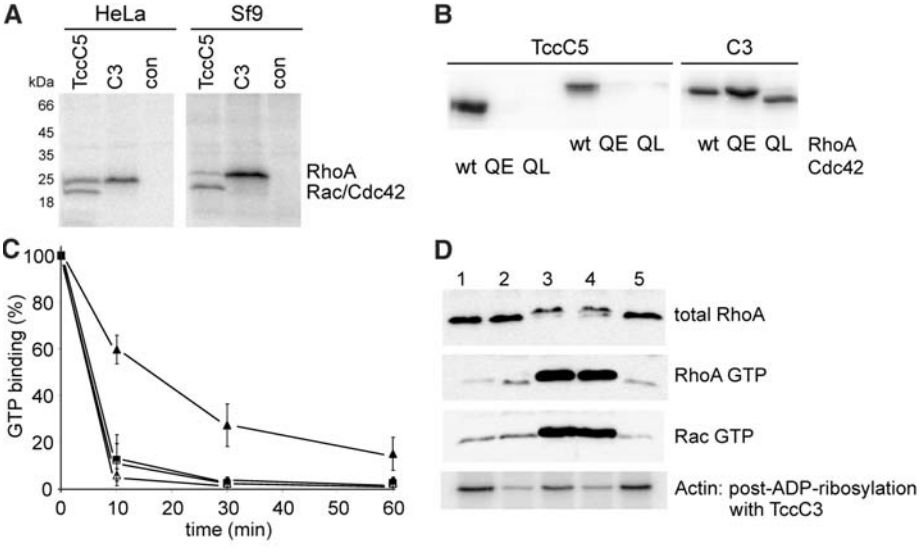

Fig. 3. ADP-ribosylation by TccC5. (**A**) Lysates of serum-starved HeLa or Sf9 cells or (**B**) recombinant GTPases (Cdc42 and RhoA) and indicated mutants (RhoAQ63E, RhoAQ63L, Cdc42Q61E, and Cdc42Q61L) were [^{32}P]ADP-ribosylated by TccC5, *C. botulinum* exoenzyme C3 (C3), or buffer (control). Labeled proteins were analyzed by means of SDS-PAGE and phosphorimaging. (**C**) Influence of TccC5-induced ADP-ribosylation of Cdc42 on GTP hydrolysis. Recombinant Cdc42 was incubated with TccC5 (▲, Δ) or the inactive N-terminal part of TccC5 (■, □) with (▲, ■) or without (Δ, □) NAD$^+$ for 1 hour. Then, the GTPase was loaded with [γ-^{32}P]GTP. Remaining nonhydrolyzed GTP bound to Cdc42 was measured with a filter binding assay. Data are percentage of initial loading (mean ± SD, n = 3 independent experiments). (**D**) Toxin effects on Rho GTPases and actin. Intact HeLa cells were treated without (lane 1) or with PTC3 (lane 2), PTC5 (lane 3), PTC3 and PTC5 (lane 4), or TcdA1 alone (lane 5) for 3 hours. Thereafter, RhoA was detected in cell lysates by means of immunoblotting (top, total RhoA). Activation of RhoA and Rac was analyzed through pull-down with rhotekin- and PAK-coupled beads, respectively. Bound GTPases were detected by means of immunoblotting. (Bottom) Each lysate was post–ADP-ribosylated with TccC3 with [^{32}P]NAD$^+$. Radio-labeled actin was analyzed by means of SDS-PAGE and autoradiography.

GTPases (*17*). Accordingly, ADP-ribosylation of Rho GTPases by TccC5 inhibited the GTP hydrolysis catalyzed by the GTPases (Fig. 3C and fig. S8C). Thus, TccC5 may cause persistent activation of Rho GTPases by ADP-ribosylation. To confirm that the toxins caused selective modification of target proteins in intact cells, we treated HeLa cells with PTC3 or PTC5 and also with the combination of PTC3 and PTC5. As an additional control, cells were treated with TcdA1 only. Thereafter, activated RhoA and Rac proteins were identified in lysates of these cells by rhotekin and PAK pull-down assays. Furthermore, actin was ADP-ribosylated in the cell lysates by TccC3 and [^{32}P]NAD^{+}. Treatment of cells with PTC3 caused ADP-ribosylation of actin, which was detected by the reduction of radioactive labeling of actin by TccC3 but no activation of Rac or RhoA (Fig. 3D). PTC5 caused activation of RhoA and Rac but did not modify actin. In the presence of PTC3 and PTC5, both activation of RhoA and Rac and ADP-ribosylation of actin was determined. As expected, TcdA1 alone did not activate Rho GTPases or modify actin. Thus, PTC5 activates Rho GTPases in intact cells. Activation of RhoA is probably the reason for massive formation of stress fibers. RhoA activation by PTC5 also occurs in Sf9 insect cells (fig. S8B).

Here, we have elucidated the causal mechanisms of the alterations of the actin cytoskeleton induced by the Tc toxins and suggest a model for the mode of action of the toxins [supporting online material (SOM) text and fig. S10]. Both TccC3 and TccC5, which enter the target cell cytosol via TcdA1, ADP-ribosylate actin and Rho-GTPases, respectively. The toxins thus cause actin clustering by means of a concerted action. TccC3 releases actin from its thymosin-β4 complex, probably supplying monomeric actin to the filament-promoting activities of profilin and actin nucleators such as the formins (*18*, *19*), and TccC5 activates signal pathways, which support stress fiber formation. In addition, because Rho GTPases are also involved in a large array of other biological functions (*20*, *21*), their alteration by Tc toxins may be of major importance for the host-pathogen interaction of *P. luminescens*. Tc toxins are a common principle in insect pathogenicity of a broad spectrum of bacteria and have been identified in human pathogenic *Yersinia pseudotuberculosis* and *Yersinia pestis* (*22*, *23*). Thus, the molecular mechanism of the prototypical Tc complexes aids the understanding of other types of Tc toxins in insecticidal bacteria and potentially human pathogens.

References and Notes

1. S. A. Joyce, R. J. Watson, D. J. Clarke, *Curr. Opin. Microbiol.* **9**, 127 (2006).
2. R. H. ffrench-Constant *et al.*, *FEMS Microbiol. Rev.* **26**, 433 (2003).
3. N. R. Waterfield, D. J. Bowen, J. D. Fetherston, R. D. Perry, R. H. ffrench-Constant, *Trends Microbiol.* **9**, 185 (2001).
4. D. Bowen *et al.*, *Science* **280**, 2129 (1998).
5. S. C. Lee *et al.*, *J. Mol. Biol.* **366**, 1558 (2007).
6. N. Waterfield, M. Hares, G. Yang, A. Dowling, R. ffrench-Constant, *Cell. Microbiol.* **7**, 373 (2005).
7. Materials and methods are available as supporting material on *Science* Online.
8. R. J. Fieldhouse, A. R. Merrill, *Trends Biochem. Sci.* **33**, 546 (2008).
9. H. Barth, K. Aktories, M. R. Popoff, B. G. Stiles, *Microbiol. Mol. Biol. Rev.* **68**, 373 (2004).
10. K. Aktories *et al.*, *Nature* **322**, 390 (1986).
11. K. Aktories, A. Wegner, *J. Cell Biol.* **109**, 1385 (1989).
12. E. Irobi *et al.*, *EMBO J.* **23**, 3599 (2004).
13. E. M. De La Cruz *et al.*, *Biophys. J.* **78**, 2516 (2000).
14. H. Q. Sun, K. Kwiatkowska, H. L. Yin, *Curr. Opin. Cell Biol.* **7**, 102 (1995).
15. M. Vogelsgesang, A. Pautsch, K. Aktories, *Naunyn Schmiedebergs Arch. Pharmacol.* **374**, 347 (2007).
16. G. Schmidt *et al.*, *Nature* **387**, 725 (1997).
17. I. R. Vetter, A. Wittinghofer, *Science* **294**, 1299 (2001).
18. M. Pring, A. Weber, M. R. Bubb, *Biochemistry* **31**, 1827 (1992).
19. S. Romero *et al.*, *Cell* **119**, 419 (2004).
20. A. B. Jaffe, A. Hall, *Annu. Rev. Cell Dev. Biol.* **21**, 247 (2005).
21. K. Burridge, K. Wennerberg, *Cell* **116**, 167 (2004).
22. J. Parkhill *et al.*, *Nature* **413**, 523 (2001).
23. M. C. Hares *et al.*, *Microbiology* **154**, 3503 (2008).
24. H. G. Mannherz *et al.*, *J. Mol. Biol.* **366**, 745 (2007).

25. We thank Agilent Technologies for supporting us with instrumentation, R. S. Goody (Dortmund, Germany) for help in stopped-flow measurements, and M. Geyer (Dortmund, Germany) for providing profilin. The study was financially supported by the Deutsche Forschungsgemeinschaft DFG to K.A. and H.G.M.

Supporting Online Material

www.sciencemag.org/cgi/content/full/327/5969/1139/DC1
Materials and Methods
SOM Text
Figs. S1 to S10
References

11 November 2009; accepted 22 January 2010
10.1126/science.1184557

Noise Can Induce Bimodality in Positive Transcriptional Feedback Loops Without Bistability

Tsz-Leung To and Narendra Maheshri*

Transcriptional positive-feedback loops are widely associated with bistability, characterized by two stable expression states that allow cells to respond to analog signals in a digital manner. Using a synthetic system in budding yeast, we show that positive feedback involving a promoter with multiple transcription factor (TF) binding sites can induce a steady-state bimodal response without cooperative binding of the TF. Deterministic models of this system do not predict bistability. Rather, the bimodal response requires a short-lived TF and stochastic fluctuations in the TF's expression. Multiple binding sites provide these fluctuations. Because many promoters possess multiple binding sites and many TFs are unstable, positive-feedback loops in gene regulatory networks may exhibit bimodal responses, but not necessarily because of deterministic bistability, as is commonly thought.

When a cell must unambiguously commit to a particular gene expression program, often a digital change occurs in a key regulator's expression (*1*). Decision-making circuitry within metabolic (*2*), developmental (*3*), and synthetic gene regulatory networks (*4*–*6*) uses positive feedback to provide bimodal, "all-or-none" expression of a regulator. The bimodal population response has been explained with deterministic models that predict bistable gene expression (*7*). Consider a positive-feedback loop where a transcriptional activator binds its own promoter to regulate expression. The open-loop promoter response (in the absence of feedback) is modeled by a Hill-type equation, where the Hill coefficient describes whether the response is linear (Hill coefficient = 1) or sigmoidal (Hill coefficient > 1) before saturating. The basis for sigmoidal responses can be direct cooperative binding of transcription factors (TFs) to promoters, or indirect cooperativity via nucleosome displacement (*8*). Without cooperativity, bistability is not predicted.

To understand how promoter structure relates to the Hill coefficient, we used the widely used tet-Off system, adapted for budding yeast (*9*). The tet–transcriptional activator (tTA) binds to a tet operator (tetO) sequence in the absence of doxycycline. We constructed yeast strains without (open loop) and with feedback (closed loop), using previously designed promoters with one (1xtetO) and seven (7xtetO) binding sites (*9*). With 1xtetO in positive feedback, the reporter exhibits a graded steady-state response to changes in feedback strength, whereas 7xtetO exhibits a bimodal response (Fig. 1A). One explanation is that 7xtetO has a sigmoidal open-loop response due to cooperative binding of tTA to multiple binding sites, resulting in bistability (*6*, *10*). Yet, if one accounts for the binding of doxycycline to the tTA dimer [Supporting Online Material (SOM) Text], both 1xtetO and 7xtetO exhibit a noncooperative open-loop response, with a Hill coefficient of ~1 (Fig. 1B). To eliminate the possibility of altered doxycycline binding, we titrated tTA levels directly, using a galactose-inducible promoter, and confirmed the

Department of Chemical Engineering, Massachusetts Institute of Technology, Cambridge, MA 02139, USA.

*To whom correspondence should be addressed. E-mail: narendra@mit.edu